

## Supporting Information

### File 1

#### **Tunneling Ultramicroelectrode (T-UME): Nanoelectrodes and Nanoparticle Collisions**

Jiyeon Kim, Byung-Kwon Kim, SungKi Cho and Allen J. Bard\*

*Center for Electrochemistry, Department of Chemistry, The University of Texas at Austin, Austin, Texas, 78712*

Experimental details

#### **Reagents**

Hydrogen hexachloroplatinate hydrate ( $\text{H}_2\text{PtCl}_6 \cdot \text{H}_2\text{O}$ ) and citric acid were obtained from ACROS organic. Potassium ferrocyanide ( $\text{K}_4\text{Fe}(\text{CN})_6$ ), sodium chloride (NaCl) and potassium ferrocyanide ( $\text{K}_3\text{Fe}(\text{CN})_6$ ) were purchased from Fisher Scientific. Ferrocenemethanol (97%, FcMeOH), titanium trichloride ( $\text{TiCl}_3$ ), sodium citrate, L-ascorbic acid, and sodium borohydride were obtained from Sigma-Aldrich. All chemicals were used as received. Millipore water ( $>18\text{M}\Omega\text{-cm}$ ) was used in all experiments. All electrolyte solutions for electrochemical measurements were additionally filtrated with  $0.22\ \mu\text{m}$  pore sized Millex filter unit (Merck Millipore Ltd., Germany).

#### **Preparation of $\text{TiO}_2$ Deposited Pt UME**

The Pt UMEs were prepared according to a procedure reported elsewhere by laser pulling (Sutter Instruments)<sup>S1</sup> followed by milling with focused ion beam (FEI Strata™ DB235 dual beam SEM/FIB). The radius of the Pt UME was checked electrochemically by cyclic voltammetry in 1 mM FcMeOH, 0.2 M NaCl solution, which was consistent with that measured by SEM. Before  $\text{TiO}_2$  deposition, the Pt UME was cleaned with piranha solution.  $\text{TiO}_2$  films were prepared on the Pt UME by anodic oxidative hydrolysis of aqueous 50 mM  $\text{TiCl}_3$  solutions at pH  $-2.30 \pm 0.05$  at (open circuit potential (OCP) + 20) mV vs. Ag/AgCl. More detailed information can be found

elsewhere.<sup>S2</sup> After each deposition step, the electrode was moved to 1 mM FcMeOH, 0.2 M NaCl solutions and checked by CV to confirm the deposition of TiO<sub>2</sub> oxo-polymer film. The deposition procedure was repeated until the CV in 1 mM FcMeOH showed indiscernible faradaic current. Subsequently, the Pt UME was dried in the atmosphere at room temperature for 1 day, undergoing dehydration to obtain the TiO<sub>2</sub> film. For the XPS characterization, TiO<sub>2</sub> film was deposited on Pt foil using the same procedure.

### The XPS Analysis of TiO<sub>2</sub> Deposited Pt Foil

Because of the technical difficulty with mounting the UME on the XPS stage, the TiO<sub>2</sub> was deposited on Pt foil instead of on a Pt UME. The binding energy peaks at 459.4 eV and 465.2 eV corresponding to 2p<sub>3/2</sub> and 2p<sub>1/2</sub> orbitals of Ti(IV) indicate that the deposited film is largely TiO<sub>2</sub> (Figure S1).<sup>S3</sup>

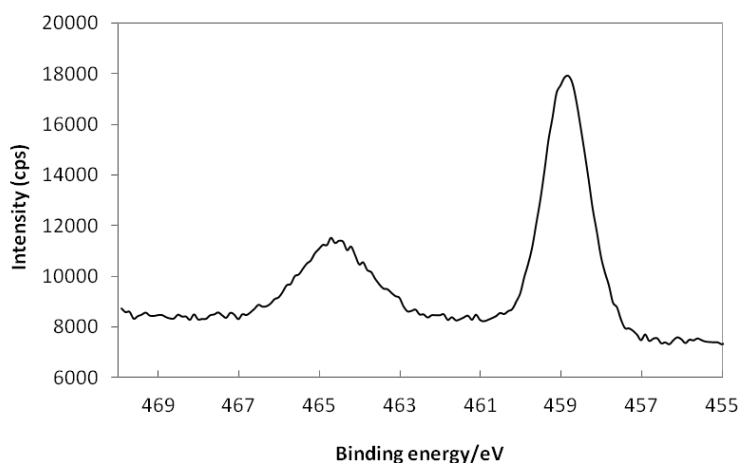


**Figure S1.** XPS spectrum of TiO<sub>2</sub> surface phase in the Ti 2p core level region. TiO<sub>2</sub> film was deposited on the Pt foil.

### Preparation of Pt Nanoparticles (NPs)

Pt NPs were prepared according to Bigall et al.<sup>S4</sup> Briefly, the Pt NP seed (diameter 4 nm) solution was prepared first. 7 mL of 3.8 mM H<sub>2</sub>PtCl<sub>6</sub>·6H<sub>2</sub>O was added to 90 mL of boiled deionized water. After 1 min, 2.2 mL of 1% sodium citrate and 0.05% citric acid was added, followed by the addition of 1.1 mL of a freshly prepared sodium borohydride (0.08%) solution

containing 1% sodium citrate and 0.05% citric acid. After 10 min, the product was cooled down to room temperature.

The larger diameter of Pt NPs was prepared using the prepared seeds. 1 mL of Pt seed was added to 29 mL deionized water at room temperature. Then, 0.045 mL of 0.4 M  $\text{H}_2\text{PtCl}_6 \cdot 6\text{H}_2\text{O}$  was added followed by the addition of 0.5 mL of a solution containing 1% sodium citrate and 1.25% L-ascorbic acid. The temperature was increased to boiling point at  $\sim 10^\circ\text{C}/\text{min}$ . The reaction time was 1 h once the temperature reached  $90^\circ\text{C}$ . To obtain the Pt NP larger than 30 nm diameter, the particles described above were used as seeds. With nanoparticle tracking analysis, using NanoSight (model NS500, Malvern Ins. Co.), the size distribution of synthesized Pt NPs was characterized. We used Pt NP with ca. 52 nm ( $52 \pm 30$  nm) diameter for the electrochemistry.

### **Instrumentation**

The electrochemical measurements were performed using a CHI model 920C potentiostat (CH Instruments, Austin, TX) with the two-electrode cell placed on a grounded stage. The bandwidth of the potentiostat is 1MHz. The used filter setting for the CV measurement was 150 Hz for potential filter, 32 Hz for i/E converter filter, 15 Hz signal filter, 32 Hz for 2<sup>nd</sup> order i/E filter, and 15 Hz for 2<sup>nd</sup> order signal filter. For the chronoamperometric measurements, the filter setting was 32 Hz for i/E converter filter, 150 Hz for signal filter, 32 Hz for 2<sup>nd</sup> order i/E filter, and 150 Hz for 2<sup>nd</sup> order lower pass filter for signal. Ag/AgCl in a saturated KCl solution was used as a reference and counter electrode. The SEM image was obtained using dual beam instrument (FEI Strata™ DB235 dual beam SEM/FIB). Synthesized Pt nanoparticle was characterized by nanoparticle tracking analysis using NanoSight (model No. NS500, Malvern Ins. Co.).  $\text{TiO}_2$  deposition film was characterized by X-ray photoelectron spectroscopy (Kratos XPS, Kratos Analytical Ltd., UK) equipped with a monochromatic Al X-ray source. For SECM approach curve measurements, a video-microscope (CCD camera (Infinity2-1), Caltex lens (VZ-400)) was used.

### **The Characterization of Size Distribution of Synthesized Pt NPs by Nanoparticle Tracking Analysis with NanoSight**

The synthesized Pt NP solution was characterized by nanoparticle tracking analysis (NTA). NTA analyzes the particles in liquids by illuminating individual NPs by light scattering with laser light. They are imaged and their Brownian motion is tracked, which allows determination of the particle size. The light scattered by the particles is captured using a scientific digital camera and the motion of each particle is tracked from frame to frame, thus the rate of particle movement is related to a sphere equivalent hydrodynamic radius as calculated through the Stokes-Einstein equation. The detection limit of Pt NPs is about 10 nm, so sizes below this limit are not represented in the distribution; the upper limit is 2000 nm. Since our Pt NP synthesis starts from Pt NP seeds of about 4 nm diam., the final distribution with an average of about 52 nm diam. Pt NPs includes some unreacted seed NPs, which cannot be detected by the NanoSight. However, a 5 nm diam. Pt NP is large enough to be seen by the tunneling on the TiO<sub>2</sub> deposited Pt UME in the reduction of 10 mM Fe(CN)<sub>6</sub><sup>3-</sup>.

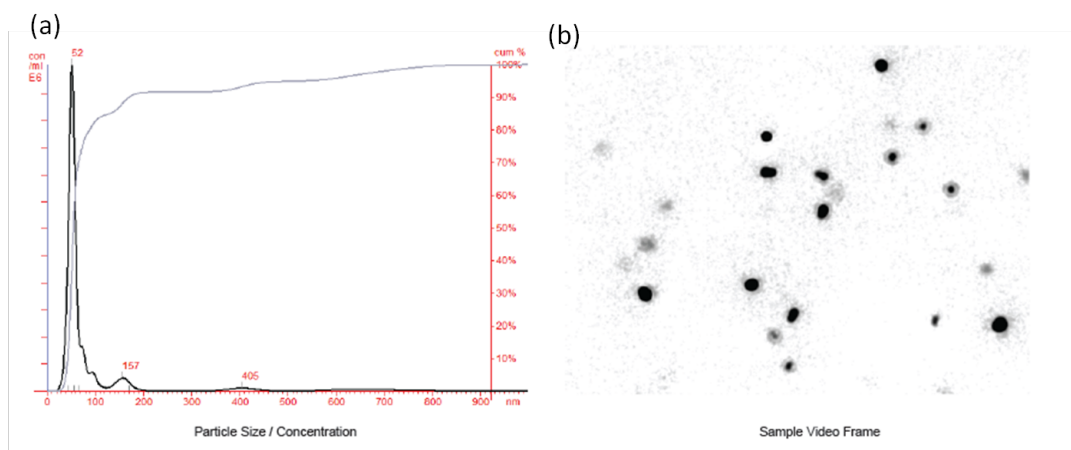


**Figure S2.** (a) Size distribution of synthesized Pt NP and (b) visualized Pt NP captured in the video frame by NanoSight. Note that Pt NPs smaller than about 10 nm were not imaged and do not appear in the distribution in (a).

### The Estimation of TiO<sub>2</sub> Film by Measuring the Capacitance

To obtain the thickness information of prepared TiO<sub>2</sub> film, we applied Gouy-Chapman-Stern theory to Pt UME/ TiO<sub>2</sub> in contact with an electrolyte solution.<sup>S5,S6,S7</sup> The total capacitance ( $C_T$ ) of Pt UME/ TiO<sub>2</sub> includes the capacitance of the TiO<sub>2</sub> film ( $C_{TiO_2}$ ) connected in series with capacitance of the Stern and diffuse layers ( $C_S$ ,  $C_D$ , respectively), thus  $C_T$  can be expressed by

$$\frac{1}{C_T} = \frac{1}{C_{TiO_2}} + \frac{1}{C_S} + \frac{1}{C_D} \quad (1)$$

$C_{TiO_2}$ ,  $C_s$  and  $C_D$  are described by

$$\frac{1}{C_{TiO_2}} = \frac{1}{\epsilon_{TiO_2}\epsilon_0} d \quad (2)$$

$$\frac{1}{C_s} = \frac{1}{\epsilon\epsilon_0} \chi_2 \quad (3)$$

And

$$\frac{1}{C_D} = \left[ \frac{FA}{RT} \left( 1 + \frac{\sigma_M^2}{4A^2} \right)^{1/2} \right]^{-1} \quad (4)$$

where  $\epsilon_{TiO_2}$  is the dielectric constant for  $TiO_2$  film with the permittivity of free space ( $8.8542 \times 10^{-12}$  F/m),  $\epsilon_0$ , the  $TiO_2$  film thickness,  $d$ , the dielectric constant for the electrolyte solution,  $\epsilon$ , and the Stern layer thickness,  $\chi_2$ .  $A$  is equal to  $(2RT\epsilon_0\epsilon c_{elec})^{1/2}$ , where  $c_{elec}$  is the electrolyte concentration with gas constant,  $R$  and temperature,  $T$ .  $\sigma_M$  is the charge density on the electrode.  $C_T$  can be estimated from 20 of CV measurements at 50 mV/s with 10 different  $TiO_2$  deposited electrodes in 10 mM  $K_3Fe(CN)_6$  in the absence of Pt NP by,

$$C_T = \frac{q_s}{\psi_{max} - \psi_{min}} \quad (5)$$

where,  $q_s$  is the charge per unit surface area, accumulated at the electrode surface during one cycle, thus calculated by integrating the current density at the electrode surface with respect to time.  $\psi_{max} - \psi_{min}$  is referred to as potential window, 0.5 V from 0.5 V to 0 V. Two representative CVs are shown in Figure S3 with 200 nm radius Pt UME/ $TiO_2$ ,  $40 \pm 10$  fA of capacitive current was observed with 25 fA noise. The measured  $C_T$  and calculated  $C_s$  and  $C_D$  were  $1.25 \pm 0.35$  F/m<sup>2</sup>, 2.10 F/m<sup>2</sup> and 5.26 F/m<sup>2</sup>, respectively. As a result, the estimated thickness of  $TiO_2$  film varies 1.0 to 2.2 nm using 50 or 110 of  $\epsilon_{TiO_2}$  for anatase or rutile  $TiO_2$ , but the uncertainties in the appropriate  $\epsilon_{TiO_2}$  and the other corrections make these numbers considered approximate. In

addition, the small level of the measured capacitance could be in the measurement error range, thus more precise measurement for the capacitance will be done by the electrochemical impedance microscopy, later.

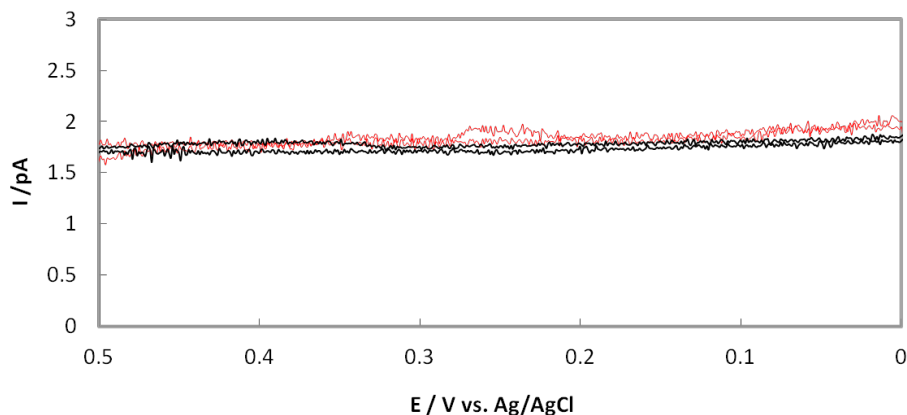


**Figure S3.** Cyclic voltammograms with Pt UME/TiO<sub>2</sub> in 10 mM Fe(CN)<sub>6</sub><sup>3-</sup> at 50 mV/s.

### The Imaging of T-UME by SEM

We could confirm the presence of the attached Pt NP on the TiO<sub>2</sub> film by SEM taken immediately after the collision experiment. Figure S4 presents two Pt NPs with ~80 nm diameter adsorbed on the Pt T-UME. Pt NP selectively adhered to the TiO<sub>2</sub> layer rather than the glass sheath. Such a stable and selective adhesion could result from the interaction between the citrate ion capping agent of Pt NPs and the TiO<sub>2</sub>. It has been reported that chemisorption can occur at TiO<sub>2</sub> through carboxylate groups in the fully deprotonated citrate ions (pK<sub>a1</sub>=3.13, pK<sub>a2</sub>=4.76, pK<sub>a3</sub>=6.40) at pH 7 act as a tridentate linkage and make a bridge to a metal of metal oxide substrate such as TiO<sub>2</sub>, or Al<sub>2</sub>O<sub>3</sub>.<sup>S8, S9, S10</sup> Moreover, we were able to observe that the attached Pt NP on T-UME after the first collision response was mostly only one or two Pt NPs attached to each other laterally. It was rare to see two Pt NPs attached vertically on the TiO<sub>2</sub> layer. This might be because of the less stable adhesion of Pt to Pt compared to the TiO<sub>2</sub> layer due to the smaller contact area than the laterally oriented adhesion during leaving from the solution and washing with DI water.

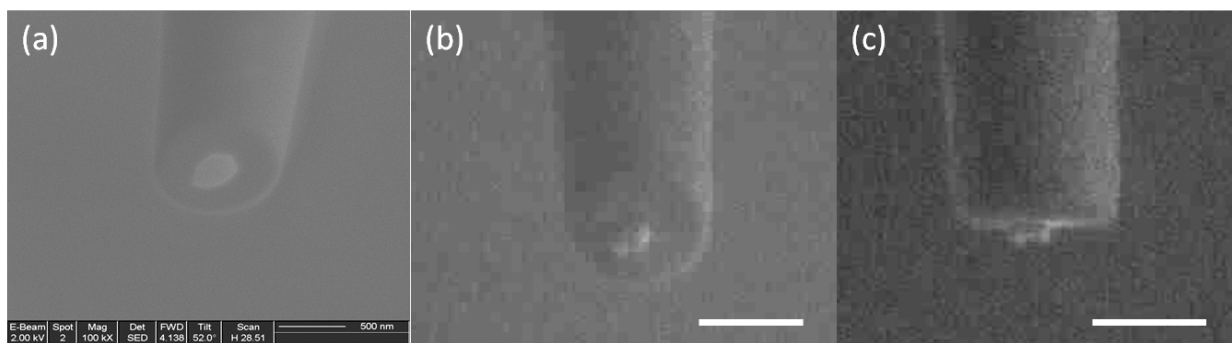


**Figure S4.** SEM images of (a) bare Pt UME and (b, c) after attachment of Pt NP on TiO<sub>2</sub> film deposited Pt UME. The scale bars equal 500 nm.

### The Measurements of SECM Approach Curves

To obtain the SECM approach curves with prepared T-UME of Pt UME/TiO<sub>2</sub>/Pt NP, the tilt of glassy carbon substrate or Si wafer substrate was adjusted with two steps. First, using the leveler, the substrate tilt was coarsely adjusted. The coarsely adjusted tilt was finely controlled using the video-microscope. Since the orientation of FIB milling was adjusted perpendicularly to the body of the Pt UME, we aligned the substrate perpendicular to the body of the Pt UME in x and y axis with the video-microscope with less than 0.1 degree offset. This procedure can align the surface of FIB milled Pt UME parallel to the substrate, thus enabling the closer approach.

Si wafer was cleaned with piranha solution and rinsed with clean DI water thoroughly before the SECM approach curve measurement. The glassy carbon plate (1 mm thick, type 2, Alfa Aesar) was chosen for the conductive substrate, since its roughness is less than 1 nm ( $0.66 \pm 0.07$  nm) as reported.<sup>S11</sup> The glassy carbon plate was lightly polished with 0.3 μm alumina, rinsed with DI water, and then lightly polished with 0.05 μm alumina again. Then, the plate was sonicated for 20 min in DI water, rinsed with DI water, and dried with Ar gas.<sup>S11</sup>

Furthermore, to avoid the electrostatic damage on the electrode surface, thereby maintaining the inlaid shape of the TiO<sub>2</sub> filmed Pt UME, we followed the method of the electrostatic damage (ESD) protection reported by Amemiya et al.<sup>S12</sup> With all the ESD damage protection, the

measurement of the SECM approach curve was carried out under the Ar purging in a humidity controlled room with higher than 30% relative humidity at 20 °C.

### **Finite Element Simulation**

SECM approach curves were simulated by solving the corresponding 2D diffusion problems using the finite element method with COMSOL Multiphysics version 4.2a (COMSOL, Inc., Burlington, MA). In this work, the inlaid electrode with sphere cap geometry was considered for inlaid TiO<sub>2</sub> deposited electrode (ii) and the attached Pt NP (iii), respectively. The model is given in Figure . An insulating or conductive substrate was considered to simulate approach curves on Si wafer or glassy carbon substrate, respectively. All dimensions were normalized by Pt NP radius. The example of the simulation for an interface with sphere Pt NP attached geometry is attached (see COMSOL report – SI File 2).

The resultant SECM approach curves are shown in Figure S6. In addition, we could simulate the negative feedback approach curve, where two Pt NPs of similar size are attached to the TiO<sub>2</sub> layer in the lateral orientation (Figure S6c). In this case, the limiting current should be significantly higher than that expected for an electrode with a single Pt NP. The approach curve, however, will give a same vertical radius as a single Pt NP, while the lateral radius gets increased. The simulated approach curve with the precise geometry leads to a single Pt NP-like behavior with an apparent radius within an error range below  $\pm 1.5\%$ . The apparent radius can be calculated from the average of two radii from the different axis. Also, the difference between the single Pt NP and laterally oriented two Pt NPs in the approach curves is smaller than 5%. In that sense, the analytical approximation would be useful to simplify the quantitative analysis of the experimental results. Overall, the fit of the experimental and the theoretical approach curves still could represent the approach of the T-UME onto the substrate for the case of either a single Pt NP or two Pt NPs.

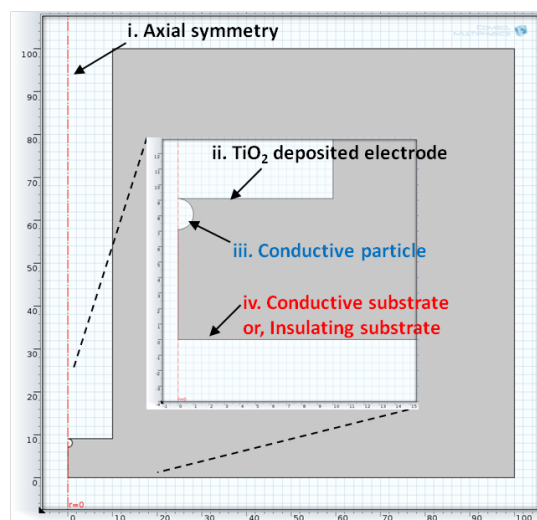


**Figure S5.** Geometry of the 2D symmetrical model used in simulations.  $\text{TiO}_2$  deposited Pt electrode disk was embedded in a glass sheath. All dimensions were normalized by the radius of conductive particle.

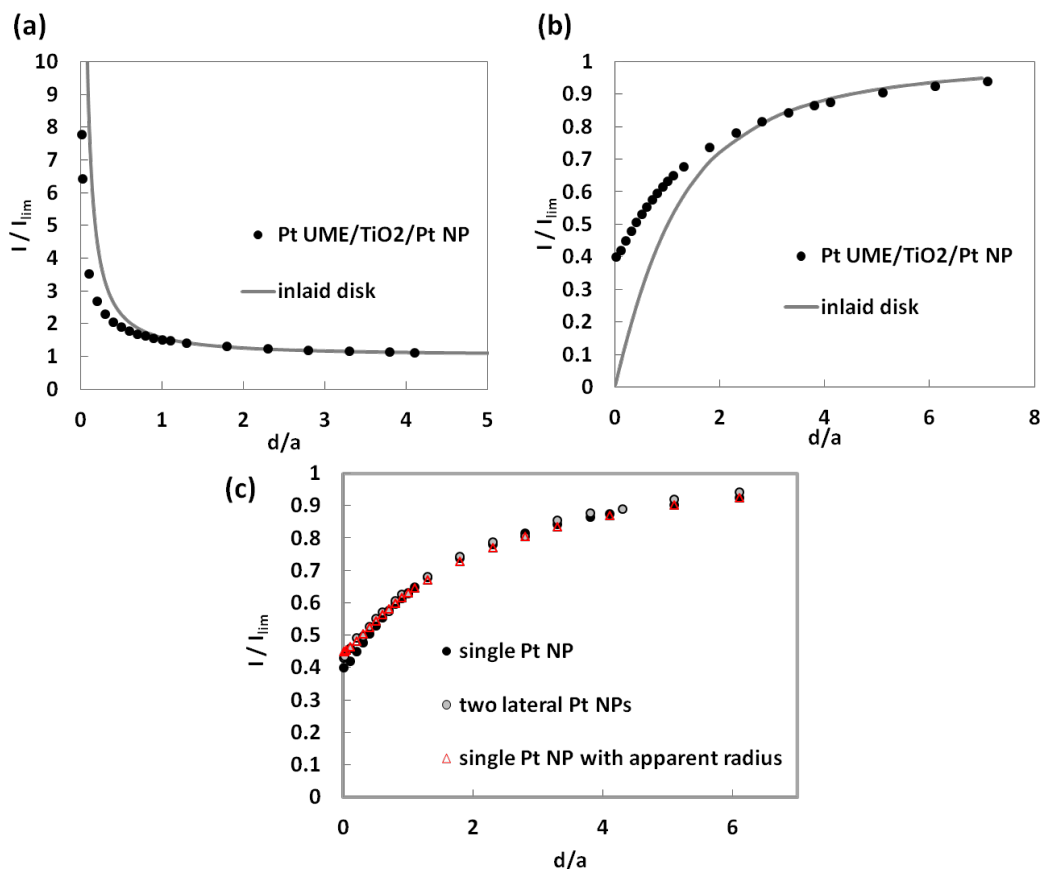


**Figure S6.** Simulated approach curves to the conductive substrate (a) and insulating substrate (b) using the finite element method. Approach curves with closed circles are with the spherical electrode, while solid lines represent approach curves with the inlaid disk electrode, respectively. (c) Simulated negative feedback approach curves with two Pt NP attached T-UME (grey circles), or a single Pt NP attached T-UME with apparent radius (red open triangles) compared to the approach curve with T-UME with a single Pt NP (black circles).

<sup>S1</sup> Kim, J.; Izadyar, A.; Nioradze, N.; Amemiya, S., *J. Am. Chem. Soc.*, **2013**, *135*, 2321-2329.

<sup>S2</sup> Kavan, L.; O'Regan, B.; Kay, A.; Grätzel, M., *J. Electroanal. Chem.*, **1993**, *346*, 291-307.

<sup>S3</sup> Ganozzi, G. et al., *J. Phys. Chem. B*, **2005**, *109*, 24411-24426.

<sup>S4</sup> Bigall, N.C.; Hrätlng, T.; Klose, M.; Simon, P.; Eng, L.M.; Eychmüller, A., *Nano. Lett.*, **2008**, *8*, 4599-4592.

<sup>S5</sup> Bard, A.J.; Faulkner, L. R., "Electrochemical Methods, Fundamentals and Applications", **2001**, 2<sup>nd</sup> edition, New York.

<sup>S6</sup> Lee, H.; Chang, B.; Kwack, W.; Jo, K.; Jeong, J.; Kwon, S.; Yang, H., *J. Electroanal. Chem.*, **2013**, *700*, 8-11.

- 
- <sup>S7</sup> Janek, R.P.; Fawcett, W.R.; Ulman, A., *J. Phys. Chem. B*, **1997**, *101*, 8550-8558.
- <sup>S8</sup> Galoppini, E., *Coord. Chem. Rev.*, **2004**, *248*, 1283-1297.
- <sup>S9</sup> Mudunkotuwa, I. A.; Grassian, V. H., *J. Am. Chem. Soc.*, **2010**, *132*, 14986-14994.
- <sup>S10</sup> Bishop, L. M.; Yeager, J. C.; Chen, X.; Wheeler, J. M.; Torelli, M. D.; Benson, M. C.; Burke, S. D.; Pedersen, J. A.; Hamers, R. J., *Langmuir*, **2012**, *28*, 1322-1329.
- <sup>S11</sup> Walker, E. K.; Vanden Bout, D. A.; Stevenson, K. J., *Langmuir*, **2012**, *28*, 1604-1610.
- <sup>S12</sup> Nioradze, N.; Chen, R.; Kim, J.; Shen, M.; Santhosh, P.; Amemiya, S., *Anal. Chem.*, **2013**, *85*, 6198-6202.